

Title:

Synaptic Location Is a Determinant of the Detrimental Effects of α -Synuclein Pathology
to Glutamatergic Transmission in the Basolateral Amygdala

Liqiang Chen^{1,5*}, Chetan Nagaraja^{1*}, Samuel Daniels^{1*}, Zoe A. Fisk²⁻⁵, Rachel Dvorak¹,
Lindsay Meyerdirk^{1,5}, Jennifer A Steiner¹, Martha L. Escobar Galvis¹, Michael X.
Henderson^{1,5}, Maxime W.C. Rousseaux²⁻⁵, Patrik Brundin⁶, Hong-Yuan Chu^{1,5}

¹Department of Neurodegenerative Science, Parkinson's Disease Center, Van Andel
Institute, Grand Rapids, MI, 49503

²Department of Cellular and Molecular Medicine, University of Ottawa, Ottawa, ON

³University of Ottawa Brain and Mind Research Institute, Ottawa, ON

⁴Ottawa Institute of Systems Biology, Ottawa, ON

⁵Aligning Science Across Parkinson's (ASAP) Collaborative Research Network, Chevy
Chase, MD, 20815

⁶Pharma Research and Early Development (pRED), F. Hoffman-La Roche, Little Falls,
NJ, USA

* These authors contributed equally to this work

Address

333 Bostwick Ave NE, Grand Rapids, MI, 49503, USA

Correspondence

Hongyuan.chu@vai.org

Acknowledgement

This work was supported by the NARSAD Young Investigator award from the Brain and Behavior Research Foundation (H.Y.C) and an investigator-initiated research award from the Department of Defense (W81XWH2110943, PI: H.Y.C). Dr. Hong-Yuan Chu is a Frederick & Alice Coles and Thomas & Nancy Coles Investigator. This research was funded in part by Aligning Science Across Parkinson's [ASAP-020625 for M.W.C.R., ASAP-020616 for M.X.H., ASAP-020572 for H.Y.C.] through the Michael J. Fox Foundation for Parkinson's Research (MJFF). For the purpose of open access, the author has applied a CC BY public copyright license to all Author Accepted Manuscripts arising from this submission. The authors thank the Van Andel Institute Optical Imaging Core for the advanced confocal microscopy as well as the Van Andel Institute Vivarium and Transgenics Core, especially Megan Tompkins, Alyssa Bradfield, Malista Powers, and William Weaver for animal husbandry and colony maintenance.

Conflicts of interest

P.B. has received support as a consultant from AbbVie, Axial Therapeutics., Calico Life Sciences, CuraSen, Enterin Inc, Fujifilm-Cellular Dynamics International, Idorsia Pharmaceuticals, Lundbeck A/S. He has received commercial support for research from Lundbeck A/S and F. Hoffman-La Roche. He has ownership interests in Acousort AB, Axial Therapeutics, Enterin Inc, Roche, and RYNE Biotechnology. During the time that this paper was undergoing revision he became an employee of F. Hoffman-La Roche, although none of the data were generated by this company.

Abstract

The presynaptic protein α -synuclein (α Syn) has been suggested to be involved in the pathogenesis of Parkinson's disease (PD). In PD, the amygdala is prone to develop insoluble α Syn aggregates, and it has been suggested that circuit dysfunction involving the amygdala contributes to the psychiatric symptoms. Yet, how α Syn aggregates affect amygdala function is unknown. In this study, we examined α Syn in glutamatergic axon terminals and the impact of its aggregation on glutamatergic transmission in the basolateral amygdala (BLA). We found that α Syn is primarily present in the vesicular glutamate transporter 1-expressing (vGluT1⁺) terminals in mouse BLA, which is consistent with higher levels of α Syn expression in vGluT1⁺ glutamatergic neurons in the cerebral cortex relative to the vGluT2⁺ glutamatergic neurons in the thalamus. We found that α Syn aggregation selectively decreased the cortico-BLA, but not the thalamo-BLA, transmission; and that cortico-BLA synapses displayed enhanced short-term depression upon repetitive stimulation. In addition, using confocal microscopy, we found that vGluT1⁺ axon terminals exhibited decreased levels of soluble α Syn, which suggests that lower levels of soluble α Syn might underlie the enhanced short-term depression of cortico-BLA synapses. In agreement with this idea, we found that cortico-BLA synaptic depression was also enhanced in α Syn knockout mice.

In conclusion, both basal and dynamic cortico-BLA transmission were disrupted by abnormal aggregation of α Syn and these changes might be relevant to the perturbed cortical control of the amygdala that has been suggested to play a role in psychiatric symptoms in PD.

Introduction

α -Synuclein (α Syn) is a soluble protein abundant at presynaptic axon terminals, where it regulates the dynamics of synaptic vesicles through interaction with synaptic proteins and presynaptic membranes (Burré et al., 2010; Runwal and Edwards, 2021; Vargas et al., 2017). α Syn is also prone to form insoluble cytoplasmic aggregates, which are the major protein component of Lewy pathology seen in synucleinopathies like Parkinson's disease (PD) (Mezey et al., 1998; Spillantini et al., 1997). Increasing evidence supports the notion that pathologic α Syn propagates between synaptically interconnected brain regions and underlies PD progression (Angot et al., 2010; Luk et al., 2012; Uemura et al., 2020).

The amygdala is a key limbic structure for emotion regulation (Janak and Tye, 2015). Compelling clinical evidence indicates that cortical control of the amygdala activity is impaired in PD, leading to an inappropriate encoding of emotion valence or deficits in linking emotion to behavior (Bowers et al., 2006; Hu et al., 2015; Yoshimura et al., 2005). Moreover, the amygdala shows selective vulnerability to Lewy pathology (Harding et al., 2002; Nelson et al., 2017; Sorrentino et al., 2019), thus an impaired amygdala network function has been proposed to underlie the disrupted emotion processing in PD patients (Harding et al., 2002). Still, the normal function of α Syn and how its aggregation can impair amygdala circuit function remain poorly understood. Here, we show that α Syn is primarily present in vesicular glutamate transporter 1-expressing (vGluT1⁺) cortical axon terminals, and, by contrast, is barely detectable in vGluT2⁺ thalamic axon terminals in the basolateral amygdala (BLA). In an α Syn preformed fibrils (PFFs) model of synucleinopathies, α Syn pathology decreases

vGluT1⁺ cortico-BLA glutamatergic transmission, without affecting the vGluT2⁺ thalamo-BLA neurotransmission. Further, we demonstrate that a partial (secondary to α Syn aggregation) or complete (*Snca* KO mice) depletion of soluble α Syn from the axon boutons promotes short-term depression at cortico-BLA synapses in response to prolonged stimulation, leading to an impaired gain control of cortical inputs to the BLA. Therefore, we conclude that both gain of toxic properties and loss of normal function of α Syn contribute to the input-specific disruption of cortico-BLA synaptic connectivity and plasticity in synucleinopathies. Our data support clinical observations of an impaired cortical control of the amygdala activity that could contribute to psychiatric deficits of PD patients.

Results

α Syn localizes preferentially in vGluT1⁺ axon terminals in mouse brain

Compelling evidence from PD patients suggests that the amygdala exhibits an impaired responsiveness to sensory stimuli, arising mainly from the cerebral cortex and the thalamus (Bowers et al., 2006; Hu et al., 2015). Thus, we examined the presence of α Syn in vGluT1⁺ and vGluT2⁺ axon boutons in WT mouse brains, which mainly come from cortical and thalamic regions, respectively (Freneau et al., 2001; Kaneko and Fujiyama, 2002; Vigneault et al., 2015). Figure 1 shows that α Syn immunoreactivity colocalizes with vGluT1⁺ puncta but is absent where there are vGluT2⁺ puncta, in the BLA, the cerebral cortex, and the striatum.

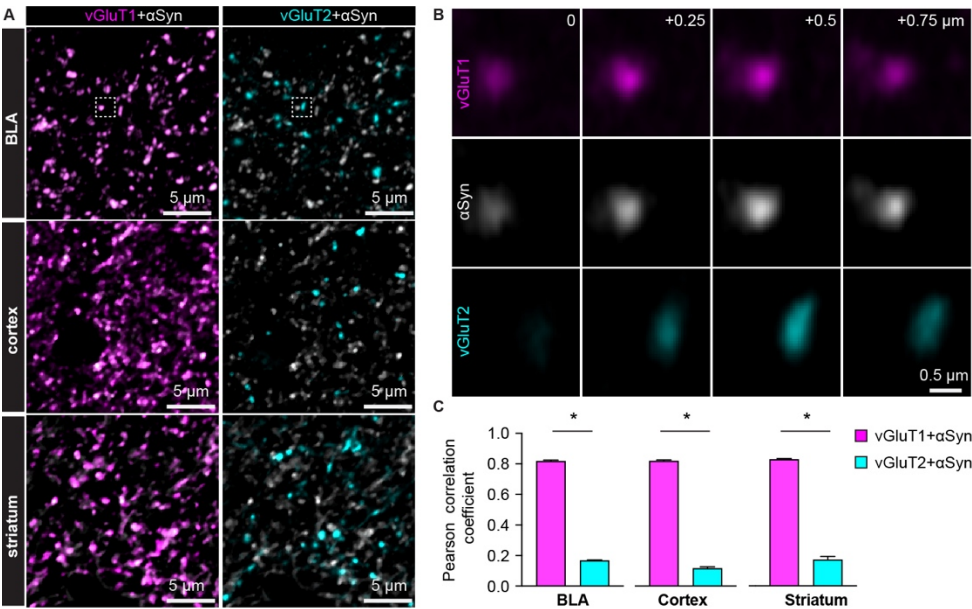


Figure 1. α Syn is selectively localized at vGluT1⁺ axon terminals in mouse brain. **A)** Representative confocal images showing colocalization of α Syn with vGluT1 (left), but not with vGluT2 (right) in the BLA (top), cerebral cortex (middle), and the striatum (bottom). Simultaneously collected confocal images from each brain region were split into vGluT1/ α Syn and vGluT2/ α Syn channels for the purpose of illustration. **B)** Zoomed z series of images of the boxed area from the BLA in (A) showing colocalization and correlated changes in the immunoreactive intensities of vGluT1 and α Syn. Such colocalization and correlation are absent between vGluT2 and α Syn within the same region. Images were taken and shown from a 0.75 μ m z-depth with an inter-section interval of 0.25 μ m. **C)** Bar graphs showing Pearson correlation coefficient between vGluT1 and α Syn, as well as between vGluT2 and α Syn, in the BLA (α Syn/vGluT1 = 0.82 ± 0.007 , α Syn/vGluT2 = 0.17 ± 0.004 ; n = 18 slices/4 mice; $p < 0.0001$, MWU), cerebral cortex (α Syn/vGluT1 = 0.82 ± 0.006 , α Syn/vGluT2 = 0.12 ± 0.009 ; n = 8 slices/3 mice; $p = 0.0002$, MWU), and the striatum (α Syn/vGluT1 = 0.83 ± 0.006 , α Syn/vGluT2 = 0.17 ± 0.02 ; n = 8 slices/3 mice; $p = 0.0002$, MWU).

Figure 1-source data 1: Source data for plot in Figure 1C.

Earlier *in situ* hybridization studies showed higher α Syn mRNA expression in the cerebral cortex and the hippocampus than in the thalamus (Abeliovich et al., 2000; Ziolkowska et al., 2005). Next, we used *Snca*^{NLS/NLS} reporter mice to determine α Syn protein localization in the cortical and thalamic areas. These mice localize endogenous α Syn to the nucleus that allows the visualization of cellular topography (Geertsma et al., 2022), circumventing the diffused α Syn immunoreactivity in WT mice (Figure 2A). We observed that the α Syn was heavily expressed in cortical layer V/VI neurons, but only moderately or barely expressed in thalamic regions, particularly in the midline thalamus that provides major excitation to the BLA (Ahmed et al., 2021; Amir et al., 2019; Hintiryan et al., 2021) (Figure 2B-D). Together, our data show that α Syn is preferentially

present at vGluT1⁺ cerebral cortical neurons and their axon terminals but is absent or expresses at very low levels at vGluT2⁺ thalamic neurons and their projections.

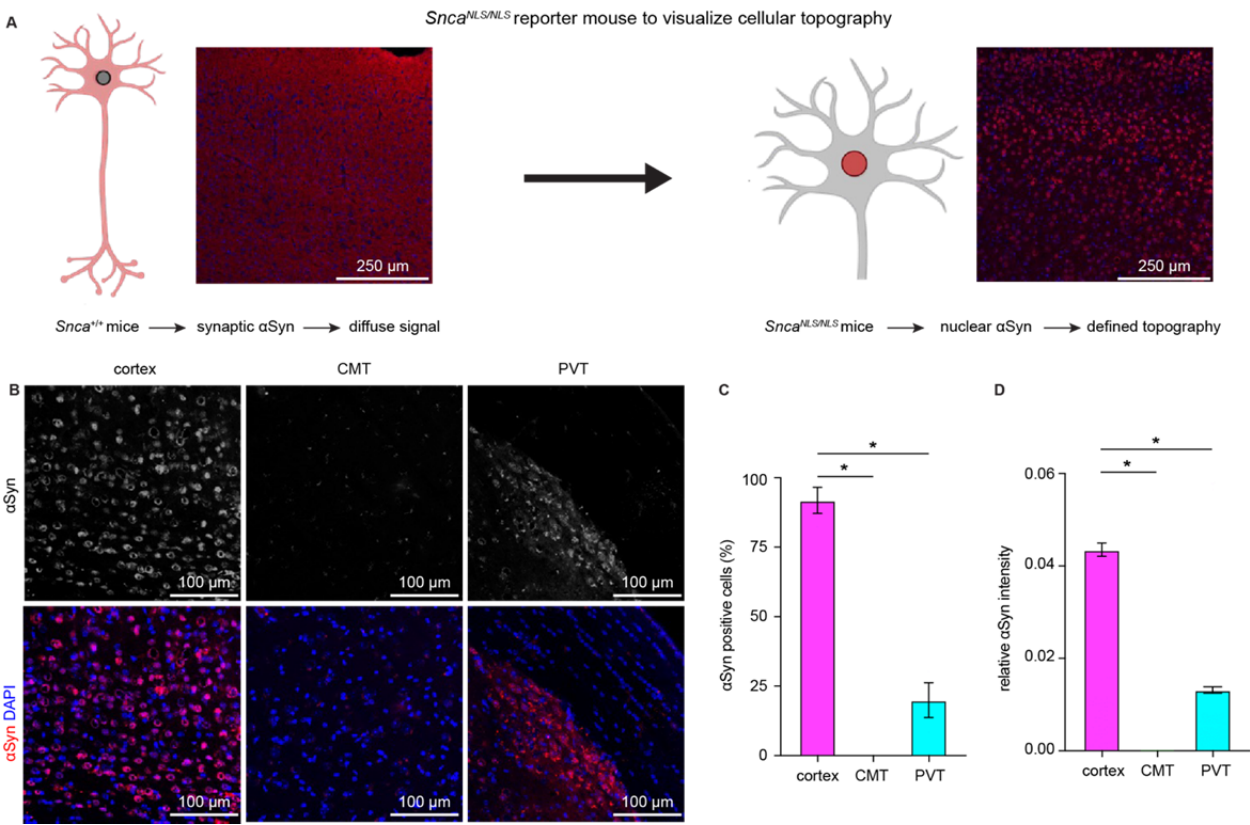


Figure 2. Cerebral cortical neurons express higher levels of endogenous αSyn than thalamic neurons. **A)** Schematic of approach to determine cellular topography of αSyn in the *Snca*^{NLS/NLS} reporter mouse line. **B)** Representative photomicrographs in the different highlighted brain regions for either αSyn alone (top panels) or co-stained with DAPI as a nuclear marker. **C-D)** Quantification of the proportion of αSyn-positive nuclei (C, %αSyn positive cells, cortex = 91.9±4.7%, CMT = 0±0%; PVT = 19.9±6.3%, n = 3 mice) or average relative intensity of αSyn in the different regions (cerebral cortex = 0.04±0.001, n = 742 cells/3 mice; CMT = 0±0, n = 364 cells/3 mice; PVT = 0.01±0.0007, n = 734 cells/3 mice). * *p* < 0.05, one-way ANOVA followed by Sidak's multiple comparison tests. Abbreviations: CMT, centromedial thalamus; PVT, periventricular thalamus.

Figure 2-source data 1: Source data for plots in Figure 2C, D.

Glutamate release from vGluT1⁺ axon terminals is selectively disrupted by α Syn pathology

Considering that the endogenous levels of α Syn are determinants of the propensity to form α Syn aggregates, we hypothesize that vGluT1⁺ neurons and their terminals are more susceptible to α Syn pathology compared to those are vGluT2⁺ (Erskine et al., 2018; Vasili et al., 2022). To test this hypothesis, we triggered widespread α Syn pathology in the brain using the intrastriatal PFFs seeding model (Luk et al., 2012). One-month post-injection, we detected robust α Syn pathology in vGluT1⁺ cerebral cortical regions (e.g., the temporal association cortex (TeA), the motor cortex, and the perirhinal cortex, Figures 3, A1-A3) and the BLA (Figures 3B-C), but we barely observed any cytoplasmic aggregates in vGluT2⁺ thalamic regions (Figures 3, A4-A5). This pattern of pathology is supported by differences in endogenous α Syn levels between the cerebral cortex and thalamus (Figure 2B-D) and consistent with earlier reports (Burtscher et al., 2019; Henderson et al., 2019; Luk et al., 2012; Stoyka et al., 2019). Importantly, neurons in the midline thalamus were retrogradely labeled when retrobeads were injected into the same location as for PFFs in the striatum (Figure 3, A6). We concluded that the absence of cytoplasmic pS129 α Syn pathology in the thalamus was not due to technical issues (i.e., missing thalamostriatal axon terminals for PFFs internalization).

Next, we focused on the BLA to assess the functional impact of α Syn aggregation on glutamatergic transmission from the cerebral cortex and thalamus (Abeliovich et al., 2000; Ziolkowska et al., 2005). We selectively activated cortical and thalamic inputs of the BLA by stimulating the external and internal capsules,

159 respectively. One-month post-injection, the amplitude of electrically evoked cortico-BLA
160 EPSCs was greatly decreased in the slices from PFFs-injected WT mice relative to
161 those from controls (Figure 3D-E). Consistently, prominent pS129 α Syn pathology can
162 be detected along the external capsule where the cortical afferents enter the BLA
163 (Figure 3B-C). In contrast, there was no difference in the amplitude of thalamo-BLA
164 EPSCs between the PFFs-injected mice and controls (Figure 3F-G).

165 To avoid potential technical issues inherent to the use of electrical stimulation,
166 we employed optogenetic approach to confirm the above results (Figure 3H-O). One-
167 month post-injection, the amplitude of optogenetically-evoked cortico-BLA EPSCs in
168 slices from PFFs-injected mice was decreased relative to those from PBS-injected
169 controls (Figure 3H-K). By contrast, we did not detect difference in the amplitude of
170 optogenetically-evoked thalamo-BLA EPSCs between groups (Figure 3L-O). Altogether,
171 we demonstrated that the presence of α Syn makes vGluT1⁺ cortical neurons and their
172 axons more vulnerable to α Syn pathology and that this pathology is associated with
173 detrimental effects on synaptic transmission.

174 Moreover, consistent with the development of α Syn pathology requiring the
175 presence of endogenous α Syn in the PFFs model (Luk et al., 2012; Volpicelli-Daley et
176 al., 2011), we did not detect difference in the cortico-BLA transmission between PFFs-
177 versus PBS-injected α Syn KO mice (Figure 3-figure supplementary 1). Furthermore,
178 because of the lack of detrimental effect in α Syn KO mice, we conclude that the
179 impaired cortico-BLA transmission in the PFFs model is likely caused by the gained
180 toxic properties of α Syn as it aggregates, instead of intrastriatal PFFs injection *per se*
181 (Cookson and Brug, 2008; Volpicelli-Daley et al., 2011).

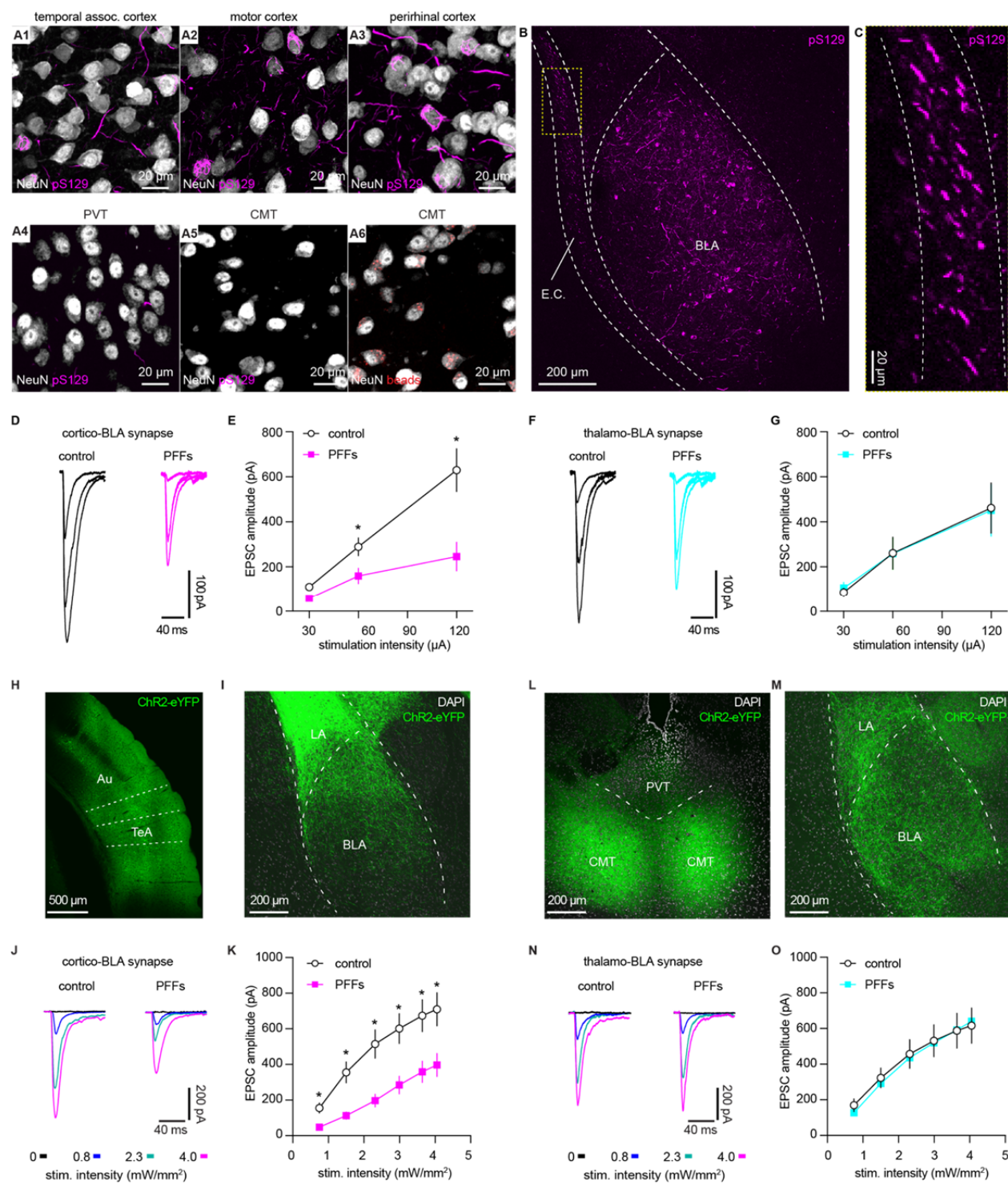


Figure 3. α Syn aggregates preferentially disrupt vGluT1⁺ cortico-BLA transmission. **A)** Representative images showing the presence of α Syn aggregates in the cortical regions (A1-A3), but largely absent in the midline thalamus (A4-A5). A6, Representative images showing retrobeads labelled neurons in the centromedial thalamus. **B-C)** Representative images showing pS129⁺ α Syn pathology in the BLA (B) and the external capsule (C). **D-E)** Representative traces of EPSCs evoked by electrical stimulation of the external capsule (D) and summarized results (E) showing a reduced cortico-BLA transmission in slices from PFFs- versus PBS-injected mice. $n = 17$ neurons/4 mice for each group. **F-G)** Representative traces of EPSCs evoked by electrical stimulation of the internal capsule (F) and summarized results (G) showing unaltered thalamo-BLA transmission in slices from PFFs- versus PBS-injected wildtype mice. $n = 17$ cells/5 mice for controls, and 13 cells/4 PFF-injected mice. **H-I)** Representative images showing viral infection site in the TeA and nearby regions (H), and the axon terminal field in the BLA (I). **J-K)** Representative traces of optogenetically-evoked EPSCs (J) and summarized results (K) showing a reduced amplitude of cortico-BLA EPSCs in slices from PFFs- versus PBS-injected mice. $n = 35-37$ neurons/4 mice per group. **L-M)** Representative images showing viral infection site in the midline thalamus (L), and the axon terminal field in the BLA (M). **N-O)** Representative traces of optogenetically-evoked EPSCs (N) and summarized results (O) showing unaltered thalamo-BLA transmission in slices from PFFs- versus PBS-injected mice. $N = 28$ neurons/4 mice per group. *, $p < 0.05$, MWU followed by Bonferroni-Dunn correction for multiple comparisons.

Figure 3-source data 1: Source data for plots in Figure 3.

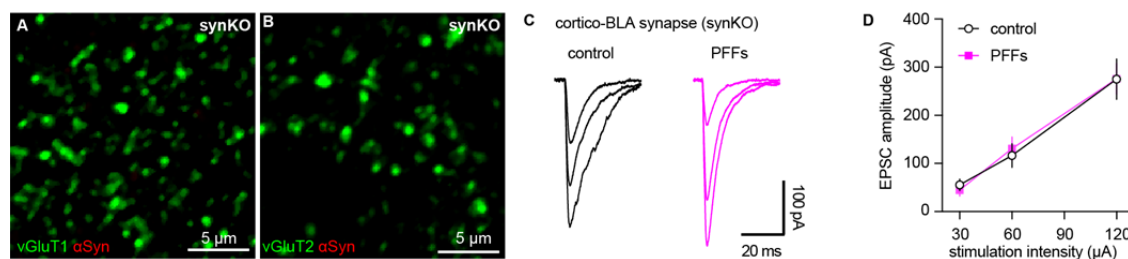


Figure 3-figure supplementary 1. Intrastratial PFFs injection does not alter cortico-BLA transmission in synKO mice. **A-B)** Representative confocal images showing lack of endogenous α Syn in vGluT1⁺ (A) and vGluT2⁺ (B) terminals in the BLA. **C)** Representative traces of EPSCs evoked by electrical stimulation of the external capsule (C) and summarized results (D) showing no changes of cortico-BLA transmission in slices from PFFs- versus PBS-injected mice. $n = 12$ neurons/3 mice for each group.

Figure 3-figure supplementary 1-source data 1: Source data for plot in Figure 3-figure supplementary 1.

α Syn pathology decreases the number of functional cortico-BLA inputs

Several mechanisms can contribute to the decreased cortico-BLA synaptic strength as α Syn pathology develops, including the loss of synapses, decreased initial release probability, and/or postsynaptic adaptations. To determine the impact of α Syn aggregation on vGluT1⁺ cortico-BLA innervation, brain sections from control and PFFs-injected mice were processed for immunohistochemical assessment of vGluT1. The density of vGluT1-immunoreactive puncta in the BLA were then determined stereologically (West, 1999). The density of vGluT1-immunoreactive puncta was not altered between PFFs- and PBS-injected mice (Figure 4A-C). These results indicate that there is no loss of cortical axon terminals or cortico-BLA synapses in PFFs-injected mice at one month post injection.

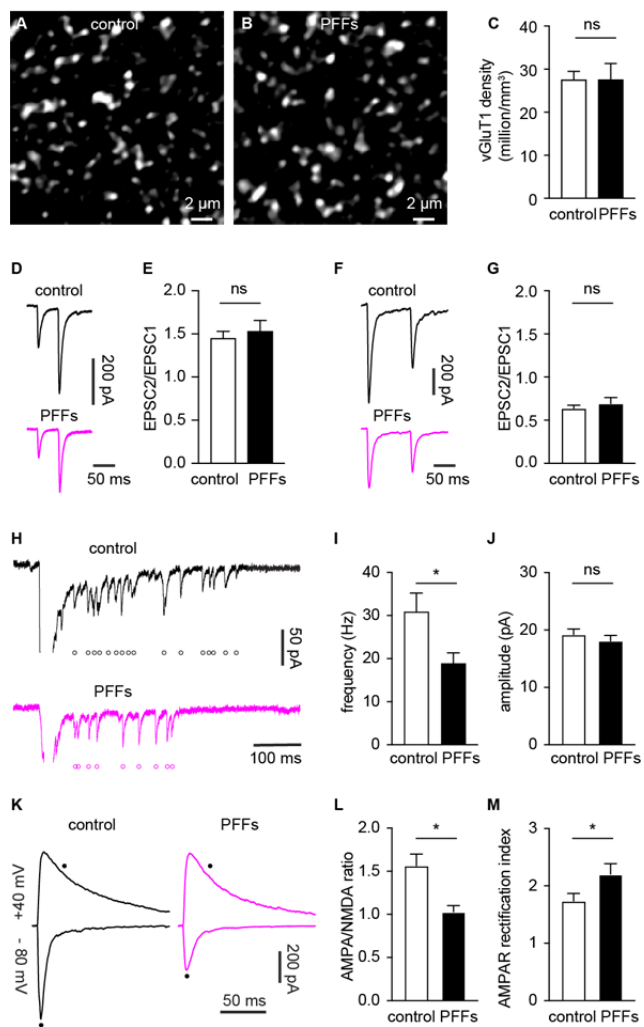


Figure 4. α Syn pathology decreases the number of functional cortico-BLA inputs. **A-B)** Representative confocal images showing vGluT1-immunoreactivity in the BLA from control (A) and PFFs-injected (B) mice. **C)** Summarized data showing no change in the vGluT1 density in the BLA between control and PFFs-injected mice (control = 27.5 ± 2 million/mm³, n = 11 slices/3 mice; PFFs = 27.5 ± 3.8 million/mm³, n = 12 slices/3 mice; $p = 0.98$, MWU). **D-E)** Representative traces of cortico-BLA EPSCs evoked by 20 Hz paired pulses of electric stimulation (D) and the summarized results of EPSC2/EPSC1 ratios (E, controls = 1.45 ± 0.08 , n = 19 neurons/4 mice; PFFs = 1.53 ± 0.13 , n = 18 neurons/4 mice; $p = 0.99$, MWU). **F-G)** Representative traces of cortico-BLA EPSCs evoked by 10 Hz paired pulses of optogenetic stimulation (F) and the summarized results of EPSC2/EPSC1 ratios (controls = 0.64 ± 0.04 , n = 35 neurons/4 mice; PFFs = 0.69 ± 0.07 , n = 31 neurons/4 mice; $p = 0.83$, MWU). **H)** Representative traces showing Sr²⁺ induced, optogenetically evoked EPSCs (Sr²⁺-EPSCs) at cortico-BLA synapses from control and PFFs-injected mice. Each open circle indicates a single identified Sr²⁺-EPSC. **I-J)** Summarized result showing a reduction of the frequency (control = 30.9 ± 4.3 Hz, n = 24 neurons/3 mice; PFFs = 18.9 ± 2.4 Hz, n = 24 neurons/3 mice; $p = 0.012$, MWU), but not the amplitude (control = 19.2 ± 0.99 pA, n = 24 neurons/3 mice; PFF = 18.1 ± 0.98 pA, n = 24 neurons/3 mice; $p = 0.31$, MWU), of Sr²⁺-EPSCs at cortico-BLA synapses. **K)** Representative cortico-BLA EPSC traces recorded at -80 mV and +40 mV from control and PFF-injected mice. Black dots indicate the time at which AMPA- and NMDA-mediated components were measured. **L)** Summarized results showing a decreased AMPA/NMDA ratio at cortico-BLA synapses from PFFs-injected mice relative to controls (control = 1.56 ± 0.13 , n = 20 neurons/3 mice; PFFs = 1.03 ± 0.07 , n = 18 neurons/3 mice, $p = 0.0012$, MWU). **M)** Summarized results showing an increased AMPA receptor rectification index at cortico-BLA synapses from PFFs-injected mice relative to controls (control = 1.74 ± 0.13 , n = 20 neurons/3 mice; PFFs = 2.21 ± 0.18 , n = 18 neurons/3 mice, $p = 0.035$, MWU). ns, not significant. *, $p < 0.05$.

Figure 4-source data 1: Source data for plots in Figure 4.

208

209

210

211

212

213

Next, we assessed functional changes of cortico-BLA synaptic transmission using electrophysiology. The initial release probability was estimated by delivering paired-pulses of electric or optogenetic stimulation of cortico-BLA synapses in control and PFFs-injected mice. Using electric stimulation approach, the ratio of EPSC2 to EPSC1 (at a 50 ms inter-pulse interval) was not altered between groups (Figure 4D-E).

Similarly, the ratio of EPSC2/EPSC1 at cortico-BLA synapses was not altered by α Syn pathology when assessed using optogenetics (at a 100 ms inter-pulse interval, Figure 4F-G). Interestingly, in contrast to the short-term facilitation in response to electric stimulation (Figure 4D-E), paired-pulses of optogenetic stimulation always led to short-term depression of cortico-BLA transmission (Figure 4F-G), which might be due to the deactivation of ChR2 itself. Together, the above data suggest that the decreased cortico-BLA transmission was not caused by a lower initial release probability.

Further, we estimated the quantal properties of cortico-BLA synapses by measuring the frequency and amplitude of Sr^{2+} -induced, optogenetically-evoked asynchronous glutamate release from cortical terminals. The frequency of optogenetically-evoked cortico-BLA asynchronous EPSCs (Sr^{2+} -EPSCs) decreased significantly, but the amplitude of cortico-BLA Sr^{2+} -EPSCs was not altered in slices from PFFs-injected mice (Figure 4H-J). Given the unaltered number of vGluT1⁺ axon terminals and initial release probability of cortico-BLA synapses, fewer readily releasable synaptic vesicles and/or release sites can explain the observed reduction in cortico-BLA transmission.

α Syn pathology decreases AMPA receptor-mediated current at cortico-BLA synapses

To determine whether the decreased cortico-BLA connection strength was associated with postsynaptic adaptations, we measured the ratio of AMPA- and NMDA-mediated EPSCs (AMPA/NMDA ratio) from the cortico-BLA synapses. In response to optogenetic stimulation, cortico-BLA inputs showed a significant reduction of AMPA/NMDA ratio in

slices from PFFs-injected mice relative to controls (Figure 4K, L). In addition, we also detected an enhanced inward rectification of AMPA-EPSCs at cortico-BLA synapses in slices from PFFs-injected mice relative to controls (Figure 4M), indicating a relatively increased contribution of GluA2-lacking, Ca^{2+} -permeable AMPA receptors to cortico-BLA transmission in PFFs-injected mice. These data suggest that αSyn pathology also triggers postsynaptic adaptations at cortico-BLA synapses. Surprisingly, we did not detect changes in the AMPA/NMDA ratio (control = 1.24 ± 0.11 , PFFs = 1.5 ± 0.12 , $n = 16$ neurons/ 3mice per group, $p = 0.15$, MWU) or AMPA receptor rectification (control = 1.12 ± 0.1 , PFFs = 1.28 ± 0.08 , $n = 16$ neurons/ 3mice per group, $p = 0.25$, MWU) from thalamo-BLA synapse between groups. Thus, the above data suggest that αSyn pathology induces input-specific decrease of postsynaptic AMPA receptor-mediated cortico-BLA transmission, instead of a global reduction of AMPA receptor function in BLA neurons.

Taken together, the development of αSyn pathology selectively decreases the functional cortico-BLA connectivity by inducing both pre- and post-synaptic adaptations and such functional changes occur prior to overt degeneration of axon terminals.

Pathological aggregation decreases αSyn levels at axon terminals and impairs short-term synaptic plasticity

Formation of cytoplasmic aggregates is believed to move soluble αSyn away from the presynaptic boutons, affecting its role in regulating synaptic vesicle pools (Benskey et al., 2016; Luk et al., 2009; Volpicelli-Daley et al., 2011). Consistent with the earlier predictions, the intensity of αSyn immunoreactivity (Syn1 antibody from BD

260 Biosciences) within vGluT1⁺ puncta decreased dramatically in slices from PFFs-injected
261 mice, leading to an increased proportion of vGluT1⁺ boutons that lack detectable level of
262 α Syn (Figure 5A-D). To avoid technical issues associated with immunostaining (e.g.,
263 antigen mask due to α Syn aggregation), we assessed the α Syn immunoreactivity within
264 vGluT1⁺ terminals using a different monoclonal antibody against mouse α Syn–Syn9027
265 (Peng et al., 2018). Consistently, both the α Syn immunoreactivity within vGluT1⁺
266 terminals and the proportion of vGluT1⁺ terminals that are α Syn-immunoreactive
267 decreased significantly in slices from PFFs-injected mice relative to controls (Figure 5E-
268 H). The percentage of α Syn-immunoreactive vGluT1⁺ terminals detected with Syn9027
269 in PFFs-injected mice was higher than those detected with Syn1, perhaps reflecting
270 differences in the exposure of their epitopes (Syn1: aa 91-99; Syn9027: aa 130-140).
271 These data suggest that α Syn pathology reduces the amount of soluble α Syn present at
272 the cortical axon terminals in the BLA, and in that way could affect its physiological
273 function.

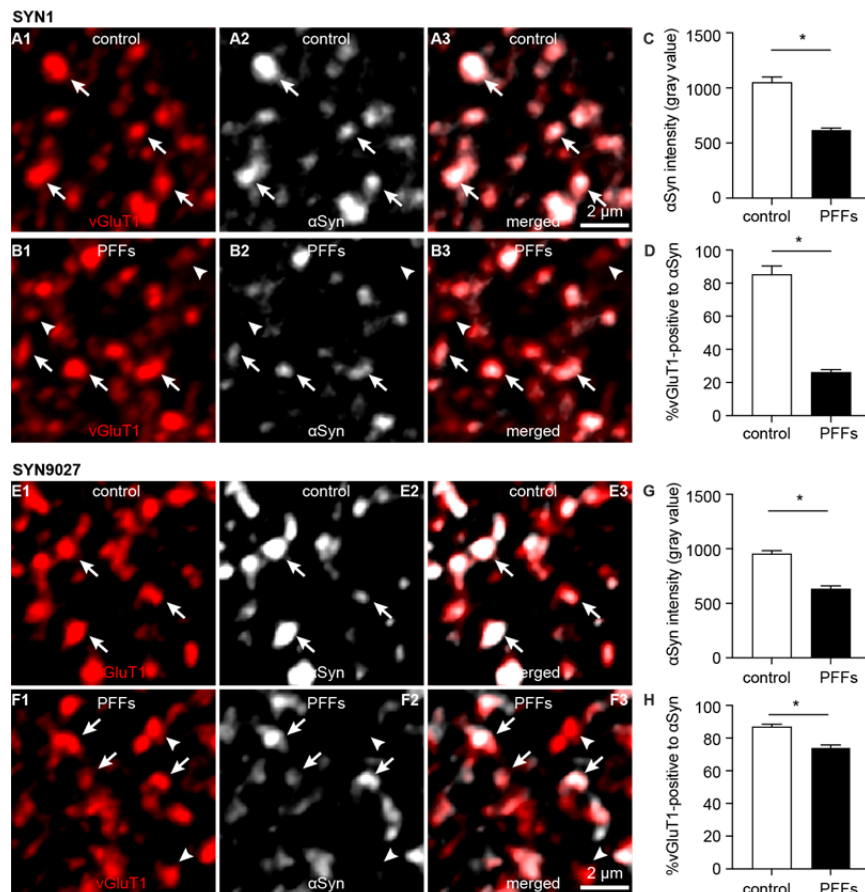


Figure 5. Decreased soluble α Syn at the axon terminals as pathology develops. A1-B3) Representative confocal images showing α Syn immunoreactivity within vGluT1⁺ puncta in the BLA using SYN1 antibody from control (A1-A3) and PFFs-injected mice (B1-B3). **C)** Summarized graph showing a reduced α Syn immunoreactivity per vGluT1 immunoreactive puncta in PFFs-injected mice relative to controls (control = 1049 ± 50 ; PFFs = 617 ± 18 , $n = 100$ puncta/group, $p < 0.0001$, MWU). **D)** Summarized graph showing a reduced percentage of vGluT1 immunoreactive puncta associated with detectable α Syn immunoreactivity in PFFs-injected mice relative to controls (controls = $85 \pm 5.2\%$; PFF = $26 \pm 1.7\%$, $n = 6$ slices/group, $p = 0.002$, MWU). **E1-F3)** Representative confocal images showing α Syn immunoreactivity within vGluT1⁺ puncta in the BLA using SYN9027 antibody from control (E1-E3) and PFFs-injected mice (F1-F3). **G)** Summarized graph showing a reduced α Syn immunoreactivity per vGluT1 immunoreactive puncta in PFFs-injected mice relative to controls (control = 954 ± 29 ; PFFs = 633 ± 27 , $n = 241$ puncta/group, $p < 0.0001$, MWU). **D)** Summarized graph showing a reduced percentage of vGluT1 immunoreactive puncta associated with detectable α Syn immunoreactivity in PFFs-injected mice relative to controls (controls = $87 \pm 1.5\%$, $n = 12$ slices; PFF = $74 \pm 1.6\%$, $n = 11$ slices, $p < 0.0001$, MWU).

Figure 5-source data 1: Source data for plots in Figure 5.

α Syn modulates the dynamics of synapse vesicle pools (Sulzer and Edwards, 2019), which plays a key role in regulating synaptic plasticity and the computational function of neural circuits (Abbott and Regehr, 2004; Alabi and Tsien, 2012). Thus, we stimulated cortico-BLA synapses repetitively to assess the impact of the observed reduction of α Syn levels on short-term synaptic plasticity. We detected a progressive depression of cortico-BLA EPSCs in control mice (Figure 6A1, A2), reflecting mainly a progressive depletion of presynaptic vesicles (Alabi and Tsien, 2012; Cabin et al., 2002). Interestingly, the cortico-BLA EPSCs in the slices from PFFs-injected mice showed a greater depression relative to those from controls (Figure 6A1, A2). These results are in line with the key role of α Syn in sustaining and mobilizing synaptic vesicle pools (Cabin et al., 2002; Sulzer and Edwards, 2019; Vargas et al., 2017), and suggest the significant impact of the loss of α Syn function on synaptic plasticity and circuit computation.

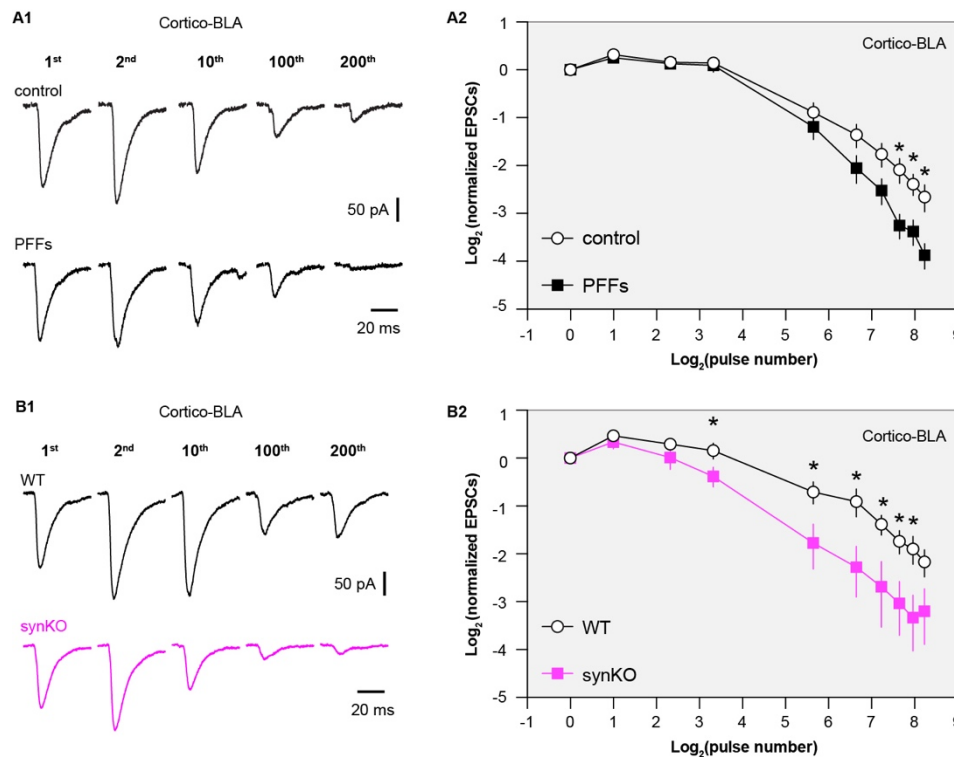


Figure 6. Loss of α Syn impairs short-term plasticity of the cortico-BLA inputs. **A1)** Representative cortico-BLA EPSCs traces from control and PFF-injected mice in response to repetitive stimulation (300 stimuli at 12.5 Hz). **A2)** Summarized graph showing the temporal profiles of cortico-EPSCs depression in slices from control and PFFs-injected mice. The cortico-BLA EPSCs from PFFs-injected mice exhibited greater reduction in the amplitude towards the end of repetitive stimulation. $n = 13-15$ neurons/ 3 mice. **B1)** Representative cortico-BLA EPSCs traces from WT control and α Syn KO mice in response to repetitive stimulation (300 stimuli at 12.5 Hz). **B2)** Summarized graph showing the temporal profiles of cortico-EPSCs depression in slices from WT control and α Syn KO mice ($n = 8-9$ neurons/3 mice. *, $p < 0.05$, MWU followed by Bonferroni-Dunn correction for multiple comparisons).

Figure 6-source data 1: Source data for plots in Figure 6.

Because both gain of toxic properties and loss of normal α Syn function are induced in the PFFs models, we employed the α Syn KO mice to further assess the impact of a loss of α Syn on the short-term synaptic plasticity of glutamatergic synapses. Consistently, the amplitude of cortico-BLA EPSCs from α Syn KO mice also exhibited greater depression in response to repetitive stimulation relative to littermate WT controls

(Figure 6B1-B2), indicating an impaired mobilization of synaptic vesicle pools. It is worth noting that the earlier onset and greater magnitude of cortico-BLA EPSC depression in α Syn KO mice versus that in PFFs-injected mice (Figure 6A-B). Thus, it is plausible that the different temporal profiles of short-term synaptic dynamics are linked to difference in the amount of α Syn present at presynaptic terminals between the PFFs model and KO mice. Last, we did not detect difference in the temporal profiles of thalamo-BLA EPSCs in slices from α Syn KO mice and those from WT controls (Figure 6-figure supplementary 1), which indicates a negligible impact of α Syn depletion on synaptic vesicle dynamics and is consistent with the lack of α Syn presence at vGluT2⁺ axon terminals (Figure 1). Together, these results suggest that pathological aggregation decreases the levels of soluble α Syn at the axon terminals, leading to a greater synaptic vesicle depletion and impaired short-term plasticity.

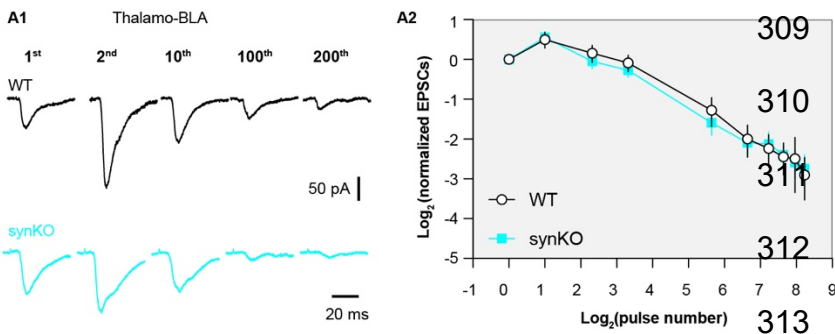


Figure 6-figure supplementary 1-source data 1: Source data for plot in Figure 6-figure supplementary 1

from WT control and α Syn KO mice in response to repetitive stimulation (300 stimuli at 12.5 Hz). **A2)** Summarized graph showing the temporal profiles of thalamo-BLA EPSCs depression in slices from WT control and α Syn KO mice (n = 9 neurons/3 mice). No statistical significance was detected between groups, MWU followed by Bonferroni-Dunn correction for multiple comparisons).

Discussion

Emerging evidence suggests that α Syn exhibit brain region- and cell type-specific expression in the brain. For example, while α Syn mRNA expression is high in glutamatergic and dopaminergic neurons, it is largely absent from GABAergic neurons across brain regions (Taguchi et al., 2015). To further explore such a cell subtype-selective α Syn expression among glutamatergic neurons and synapses, our study shows that α Syn is preferentially present at vGluT1⁺, but not vGluT2⁺, axon terminals across several brain regions, including the BLA and the striatum. Consistent with the observation from the axon terminals, we also detected higher amounts of α Syn in the cell bodies of cortical neurons relative to thalamic neurons using the recently generated *Snca*^{NLS/NLS} reporter mice (Geertsma et al., 2022). Thus, our results support a cell- and synapse-subtype-selective α Syn protein expression among glutamatergic neurons in the mouse brain.

Endogenous levels of α Syn are determinants of neuronal vulnerability to α Syn pathology. As expected, we observed a decreased in cortical, but not thalamic, inputs to the BLA neurons in a PFF-seeding model of synucleinopathies. At a relatively early-stage (i.e., 1 month post injection), α Syn pathology decreases the number of functional cortical inputs to the BLA without loss of synapse or changes in presynaptic release probability. We posit that the disrupted cortico-BLA transmission can be caused by a reduced size of readily-releasable synaptic vesicle pool and/or number of presynaptic release sites. This hypothesis was built on a wealth of evidence showing that α Syn aggregates decrease the expression of several synaptic vesicle-associated SNARE proteins (e.g., Snap25 and VAMP2) (Volpicelli-Daley et al., 2011). Moreover, our study

also suggests a decreased AMPA receptor-mediated response can underlie the impaired cortico-BLA transmission in PFFs-injected mice. On the other hand, an increased relative contribution of GluA2-lacking AMPA receptors can be a compensatory mechanism for an overall reduction in AMPA-EPSCs at cortico-BLA synapses— a hypothesis that warrants further investigation. It is worth noting that such a decreased AMPA-EPSC of BLA neurons is input specific, which selectively occurs at cortico-BLA synapses. Thus, the molecular mechanisms that cooperate pre- and post-synaptic changes at the cortical inputs, but not the thalamic inputs, remain to be defined.

Our study further highlights the dependence of regional and cellular vulnerability on the endogenous α Syn, i.e., those neurons or axon terminals that express high levels of α Syn are prone to be functionally impacted by α Syn pathology relative to those which lack of or express low levels of α Syn (Surmeier et al., 2017; Thakur et al., 2019; Vasili et al., 2022). Of particular interest is that vGluT2⁺/TH⁺ midbrain dopamine neurons and their axon terminals in the striatum have been shown to be more resilient to neurodegeneration in postmortem PD brains and animal models studies (Buck et al., 2021; Thomas et al., 2021). While several other mechanisms have been proposed (Buck et al., 2021), the absence of α Syn at vGluT2⁺ neurons/terminals could be critical for such resilience.

Loss of normal α Syn function has been thought to be an important but understudied aspect of α Syn pathology. Using an electrophysiological approach, we revealed that a partial or complete removal of α Syn from the axon terminals leads to an enhanced short-term depression in response to repetitive stimulation of cortico-BLA synapses (Figure 6). Short-term synaptic plasticity is an important “gain control”

mechanism for neurons to properly balance their responsiveness to distinct afferents in an input-specific manner (Abbott et al., 1997). Cortical and thalamic afferents of the BLA exhibit different short-term synaptic plasticity profiles *in vivo*, which could reflect their different contributions to the formation of emotion related memory and behavior (Sigurðsson et al., 2010). Physiologically, synapse-specific presence of α Syn could underlie such difference in the short-term plasticity profiles of the two inputs (Figure 1 and 6).

One can postulate that once aggregates form, a decreased synaptic strength associated with α Syn toxicity (Figure 3) and an enhanced synaptic depression due to the loss of α Syn normal function at presynaptic boutons (Figures 5 and 6) make the BLA neurons less likely to respond to sustained and repetitive sensory inputs from cortical regions. These circuit changes might explain studies showing a decreased functional connectivity of cortico-amygdala, but not the thalamo-amygdala network in PD patients, which further leads to a failed amygdala responsiveness to the aversive sensory inputs (Hu et al., 2015; Yoshimura et al., 2005).

Materials and Methods

Animals

Wild type (WT) C57Bl/6 mice (MGI Cat# 2159769, RRID:MGI:2159769) of both sexes (3-4 month-old) were obtained from the Van Andel Institute vivarium internal colony and used in the study. α Syn knockout (*Snca*^{-/-}) mice (RRID:IMSR_JAX:003692) were originally purchased from Jackson laboratories (Bar Harbor, ME) and maintained in C57Bl/6J background. Experimental *Snca*^{-/-} mice and littermate WT controls were generated from heterozygous *Snca*^{+/-} breeder pairs and were genotyped by Transnetyx (Cordova, TN, USA). *Snca*^{NLS/NLS} mice (RRID:IMSR_JAX:036763) were generated and maintained on a C57Bl/6 background as described (Geertsma et al., 2022). Mice were housed up to four animals per cage under a 12/12 h light/dark cycle with access to food and water *ad libitum* in accordance with NIH guidelines for care and use of animals. All animal studies were reviewed and approved by the Institutional Animal Care and Use Committee at Van Andel Institute (animal use protocol#: 22-02-007).

Preparation and validation of α Syn preformed fibrils

Purification of recombinant mouse α Syn and generation of α Syn preformed fibrils (PFFs) was conducted as described elsewhere (<https://www.protocols.io/view/preparation-of-fibrils-for-intracerebral-injection-bp2l6beq1gqe/v1>) (Luk et al., 2009; Volpicelli-Daley et al., 2014). The pRK172 plasmid (RRID:Addgene_166671) containing the gene of interest was transformed into BL21 (DE3) RIL-competent *E. coli* (230245, Agilent Technologies). A single colony from this transformation was expanded in Terrific Broth (12 g/L of Bacto-tryptone, 24 g/L of yeast extract 4% (v/v) glycerol, 17 mM KH₂PO₄ and

406 72 mM K₂HPO₄) with ampicillin. Bacterial pellets from the growth were sonicated and
407 the sample was boiled to precipitate undesired proteins. The supernatant was dialyzed
408 with 10 mM Tris, pH 7.6, 50 mM NaCl, 1 mM EDTA, 1 mM phenylmethylsulfonyl fluoride
409 (PMSF) overnight. Protein was filtered with a 0.22 µm filter and concentrated using
410 Vivaspin 15R 10K centrifugal filters (VS15RH01, Sartorius). Protein was then loaded
411 onto a Superdex 200 column and 2 mL fractions were collected. Fractions were run on
412 SDS-PAGE and stained with InstaBlue protein stain (50-190-5499, Fisher Scientific) to
413 select fractions that were highly enriched in αSyn. These fractions were combined and
414 dialyzed in 10 mM Tris, pH 7.6, 50 mM NaCl, 1 mM EDTA, 1 mM PMSF overnight.
415 Dialyzed fractions were applied to a MonoQ column (HiTrap Q HP 17115401,
416 Cytiva) and run using a NaCl linear gradient (0.025-1 M). Collected fractions were run
417 on SDS-PAGE and stained with InstaBlue protein stain. Fractions that were highly
418 enriched in αSyn were collected and dialyzed into DPBS (Gibco). Protein was filtered
419 through a 0.22 µm filter and concentrated to 7 mg/mL (αSyn) with Vivaspin 15R 10K
420 centrifugal filters. Monomer was aliquoted and frozen at –80°C. For preparation of αSyn
421 PFFs, αSyn monomer was shaken at 1,000 rpm for 7 days. Conversion to PFFs was
422 validated by sedimentation at 100,000 x g for 60 minutes and by thioflavin S staining.

423

424 *Stereotaxic surgery*

425 Mice were placed in a stereotaxic frame (Kopf) under 2% isoflurane anesthesia and
426 were supported by a thermostatic heating pad. Recombinant αSyn fibrils were diluted in
427 phosphate-buffered saline (PBS) to a concentration of 5 mg/ml. Prior to stereotaxic
428 injection, PFFs were pulse sonicated at medium intensity with 30 seconds on and 30

seconds off for 10 minutes using a sonicator (Biorupter Pico). To induce the formation of α Syn aggregation in mouse brain (Luk et al., 2012), sonicated PFFs (2.0 μ l) were injected bilaterally into the dorsal striatum (anteroposterior, +0.2 mm from bregma; mediolateral, \pm 2.0 mm from the midline; dorsoventral, -2.6 mm from the brain surface) using a 10- μ l syringe (Hamilton) driven by a motorized microinjector (Stoelting) at a rate of 0.2 μ l/min. Given the neuronal heterogeneity of the BLA, retrobeads (Lumafluor Inc) were diluted 10x into α Syn fibrils or PBS to label the projection neurons in the BLA for physiological studies. The final injection volume of PFFs with beads mixture was adjusted to keep a constant amount of α Syn injected across animals. Control mice received 2.0 μ l PBS or PBS with retrobeads injections in the same location. For optogenetics studies, AAV vectors encoding ChR2(H134R)-eYFP (titer = 1×10^{12} vg/ml, Addgene 26973, RRID:Addgene_127090) were stereotactically injected into and centered at the temporal association cortex (TeA) (anterioposterior -3.3 mm from the bregma, mediodorsal \pm 4.1 mm, dorsoventral -1.5 mm from the brain surface) and the midline thalamus (anterioposterior -1.5 mm from the bregma, mediodorsal 0 mm, dorsoventral -3.3 mm from the brain surface) (Ahmed et al., 2021; Amir et al., 2019). Animals were housed in their home cages before being euthanized for immunohistochemical or physiological studies at one-month post-injection. Details of this protocol can be found at: [dx.doi.org/10.17504/protocols.io.rm7vzye28lx1/v1](https://doi.org/10.17504/protocols.io.rm7vzye28lx1/v1)

Tissue collection – perfusion & sectioning. WT and *Snca*^{-/-} mice received overdosage of avertin intraperitoneally (i.p.) and were subsequently subjected to transcardial perfusion with PBS and 4% paraformaldehyde (PFA, pH 7.4). Brains were removed and post-

452 fixed in 4% PFA overnight, before being re-sectioned at 70 µm using a vibratome
453 (VT1000s, Leica Biosystems, Buffalo Grove, IL). *Snca*^{NLS/NLS} mice were anesthetized
454 with 30 µl of 120 mg/kg Euthanyl (DIN00141704) before being perfused with 10 ml 1x
455 PBS and 10 ml 4 % PFA. Brain tissue was collected and stored for 48 hours in 4% PFA.
456 Brain tissue was then dehydrated in 10, 20, and 30% sucrose solutions for 48 hours
457 each before being flash frozen in –40 °C isopentane for 1 minute. Tissues were then
458 cryosectioned at 20 µm and –21°C on the Thermo Scientific HM 525 NX cryostat at the
459 Louise Pelletier Histology Core at the University of Ottawa and stored free floating in 1x
460 PBS + 0.02 % NaN₃ at 4 °C until use. Details of this protocol can be found at:
461 [https://www.protocols.io/view/standard-operating-procedure-mouse-transcardiac-pe-](https://www.protocols.io/view/standard-operating-procedure-mouse-transcardiac-pe-3byl4b8r8vo5/v1)
462 [3byl4b8r8vo5/v1](https://www.protocols.io/view/standard-operating-procedure-mouse-transcardiac-pe-3byl4b8r8vo5/v1).

463
464 *Immunofluorescent staining.* Brain sections from WT and *Snca*^{-/-} mice were rinsed using
465 PBS and treated with 0.5% Triton X-100 and 2% normal donkey serum (MilliporeSigma)
466 in PBS for 60 min at room temperature, followed by incubation with primary antibodies
467 overnight at room temperature or for 48 hours at 4 °C. The concentrations of primary
468 antibodies were rabbit anti-pS129 αSyn (1:10,000, Abcam Cat# 1536-1,
469 RRID:AB_562180), mouse anti-αSyn (1:1,000, BD Biosciences Cat# 610787,
470 RRID:AB_398108), mouse anti-NeuN (1:2000, Millipore Cat# MAB377,
471 RRID:AB_2298772), rabbit anti-vGlut1(1:1,000, cat#: Millipore Cat# ABN1647,
472 RRID:AB_2814811) and guinea pig anti-vGluT2 (1:1000, Synaptic Systems Cat#
473 135404, RRID:AB_887884). After being thoroughly rinsed with PBS for 3 times, the
474 sections were incubated with the secondary antibodies (1:500, AlexaFluor 594 donkey

475 anti-mouse IgG, Jackson ImmunoResearch Labs Cat# 715-586-150,
476 RRID:AB_2340857; AlexaFluor 647 donkey anti-mouse IgG, Jackson ImmunoResearch
477 Labs Cat# 715-607-003, RRID:AB_2340867; AlexaFluor 488 donkey anti-mouse IgG,
478 Jackson ImmunoResearch Labs Cat# 711-546-152, RRID:AB_2340619; AlexaFluor 594
479 donkey anti-rabbit IgG, Jackson ImmunoResearch Labs Cat# 711-585-152,
480 RRID:AB_2340621, or AlexaFluor 488 donkey anti-guinea pig IgG, Jackson
481 ImmunoResearch Labs Cat# 706-545-148, RRID: AB_2340472) for 90 min at room
482 temperature. Brain sections were rinsed 3 times with PBS and mounted on glass slides
483 using Vectorshield antifade mounting medium (H-1000, Vector Laboratories) and cover
484 slipped.

485 Brain sections from *Snca*^{NLS/NLS} were incubated for 24 hours in blocking buffer
486 (1.5 % Triton X-100, 10 % cosmic calf serum in 1X PBS), 24 hours in primary Syn1
487 antibody (1:1,000, BD Biosciences Cat# 610787, RRID:AB_398108) and 1 hour in
488 secondary antibody (1:500, Alexa Fluor 568 donkey anti-mouse antibody, (Thermo
489 Fisher Scientific Cat# A10037, RRID:AB_2534013, Lot#: 1917938) with DAPI at 1:1,000
490 (Millipore Sigma, D9542-1MG). Tissue was washed in 1x PBS 5 times for 5 minutes
491 each between each treatment and mounted on Fisherbrand Superfrost Plus slides. After
492 drying for 24 hours, sections were covered with DAKO mounting medium (Cat#: S3023,
493 Lot#: 11347938) and #1.5 coverslips.

494 Details of immunofluorescent staining can be found at:
495 <https://www.protocols.io/view/immunofluorescent-staining-3b4l4bq9ovo5/v1>.

496

497 *Confocal imaging and analysis*

498 Confocal images from WT and *SNCA*^{-/-} were acquired using a Nikon A1R confocal
499 microscopy. pS129 α Syn aggregates in different brain regions were imaged under a 40x
500 objective lens. For α Syn and vGluT1/vGluT2 colocalization analysis, three synaptic
501 markers were immunostained simultaneously and z-stack images were acquired using
502 an oil immersion 100x objective (NA = 1.45; x/y, 1024 X 1024 pixels; z step = 150 nm).
503 Images were acquired using identical settings between treatment groups, including
504 laser power, pinhole size, gain, and pixel size. Intensity-based colocalization analysis
505 was performed using Imaris software (RRID:SCR_007370, version 9.3, Oxford, UK,
506 <http://www.bitplane.com/Imaris/Imaris>). Background subtraction on z-stack images was
507 conducted using ImageJ (RRID:SCR_003070, NIH, <https://imagej.net/>) prior to
508 importing files into Imaris. Once imported, two arbitrary regions of interest were created
509 using the surface function (drawing mode: circle; radius = 15 μ m; number of vertices =
510 30) and the three channels (vGluT2, vGluT1, α Syn) were masked based on the surface
511 reconstruction to isolate fluorescence within the ROIs. The Imaris "Coloc" function was
512 used to measure the colocalization between vGluT2/ α Syn and vGluT1/ α Syn for each
513 ROI. Briefly, either vGluT1 or vGluT2 was selected as channel A and α Syn was
514 selected as channel B. The automatic threshold feature within "Coloc" was used to
515 calculate the threshold values for each channel. Colocalization channels for vGluT1/
516 α Syn and vGluT2/ α Syn for each ROI were created by using the "Build Coloc Channel"
517 function. Colocalization parameters were obtained for quantification from the
518 colocalization channels. For quantification of the α Syn intensity within vGluT1⁺ axon
519 terminals, background subtraction on z-stack images was conducted using ImageJ
520 (RRID:SCR_003070, NIH, <https://imagej.net/>). After background subtraction, vGluT1

immunoreactive puncta were manually identified as a set of regions of interest (ROI, n = 20 puncta per image) from each BLA section and the mean gray values of α Syn immunoreactivity within the same ROI were then measured using ImageJ (RRID:SCR_003070, NIH, <https://imagej.net/>). Details of images analysis can be found at: [dx.doi.org/10.17504/protocols.io.n2bvj61bblk5/v1](https://doi.org/10.17504/protocols.io.n2bvj61bblk5/v1).

Confocal images from *SNCA*^{NLS/SNLS} mice were taken on the Zeiss AxioObserver Z1 LSM800 at the Cell Biology and Image Acquisition core at the University of Ottawa. Images were taken at 20x (0.8 NA) objective with 8bit 1024x1024 resolution. The following multichannel acquisition was used to detect signal: DAPI 405 nm/561nm (650V); AF568 (α Syn) 405 nm/561nm (750V). Images were analyzed using FIJI (RRID:SCR_002285, <http://fiji.sc>), where Z projected images were separated by channel and the brightness was altered (DAPI: 0-200, α Syn: 0-175). Images were then merged and exported as .jpg files.

To determine cell counts and signal intensity per region, images were inputted into Fiji as “colorized” images, then Z projected at average intensity. Images were exported as .tiff files and imported into CellProfiler Analyst 3.0 (RRID:SCR_007358, <http://cellprofiler.org>) (Stirling et al., 2021). Image metadata were extracted, and images with “C” matching 0 were assigned as DAPI, 1 assigned as α Syn. DAPI and α Syn positive cells were counted individually using the “IdentifyPrimaryObjects” feature (pixel size 20-50), and α Syn intensity was measured as “ α Syn” from “DAPI” primary object. Count and intensity data was analyzed in Prism 9 (RRID:SCR_002798, GraphPad

543 Software, <http://www.graphpad.com/>). Details of this protocol can be found at:
544 <https://www.protocols.io/private/58F47B31F3D311EC8BD90A58A9FEAC02>.

545

546 *Slice preparation for physiology.* For physiological studies, mice were deeply
547 anesthetized with avertin (300 mg/kg, i.p.) and then were perfused transcardially with
548 ice-cold, sucrose-based artificial cerebrospinal fluid (aCSF) containing (in mM) 230
549 sucrose, 26 NaHCO₃, 10 glucose, 10 MgSO₄, 2.5 KCl, 1.25 NaH₂PO₄, and 0.5 CaCl₂, 1
550 sodium pyruvate, and 0.005 L-glutathione. Next, coronal brain slices (300 µm)
551 containing BLA were prepared in the same sucrose-based aCSF solution using a
552 vibratome (VT1200S; Leica Microsystems, Buffalo Grove, IL). Brain slices were kept in
553 normal aCSF (in mM, 126 NaCl, 26 NaHCO₃, 10 glucose, 2.5 KCl, 2 CaCl₂, 2 MgSO₄,
554 1.25 NaH₂PO₄, 1 sodium pyruvate, and 0.005 L-glutathione) equilibrated with 95% O₂
555 and 5% CO₂ for 30 min at 35°C and then held at room temperature until use.

556

557 *Ex vivo electrophysiology recording and optogenetics.* Brain slices were transferred into
558 a recording chamber perfused at a rate of 3 – 4 ml/min with synthetic interstitial fluid (in
559 mM, 126 NaCl, 26 NaHCO₃, 10 glucose, 3 KCl, 1.6 CaCl₂, 1.5 MgSO₄, and 1.25 NaH₂PO₄)
560 equilibrated with 95% O₂ and 5% CO₂ at 33–34°C via a feedback-controlled in-line
561 heater (TC-324C, Warner Instruments) (Chen et al., 2021). SR-95531 (GABAzine, 10
562 µM) was routinely added extracellularly to block GABA_A receptor-mediated inhibitory
563 synaptic transmission. Neurons were visualized and recorded under gradient contrast
564 SliceScope 1000 (Scientifica, Uckfield, UK) with infrared illumination using an IR-2000
565 CCD camera (DAGE-MTI, USA) and motorized micromanipulators (Scientifica, Uckfield,

UK). Individual BLA projection neurons labeled with retrobeads were identified using a 60x water immersion objective lens (Olympus, Japan) and targeted for whole-cell patch-clamp recording. Data were collected using a MultiClamp 700B amplifier and a Digidata 1550B digitizer at a sampling rate of 50 kHz under the control of pClamp11 (RRID:SCR_011323, Molecular Devices, San Jose, USA, <http://www.moleculardevices.com/products/software/pclamp.html>). Borosilicate glass pipettes (O.D. = 1.5 mm, I.D. = 0.86 mm, item #BF150-86-10, Sutter Instruments) for patch clamp recordings (4 – 6 M Ω) were pulled using a micropipette puller (P1000, Sutter Instruments, Novato, CA).

To assess glutamatergic transmission in the BLA, glass pipettes were filled with a cesium methanesulfonate based internal solution of (in mM): 120 CH₃O₃SCs, 2.8 NaCl, 10 HEPES, 0.4 Na₄-EGTA, 5 QX314-HBr, 5 phosphocreatine, 0.1 spermine, 4 ATP-Mg, and 0.4 GTP-Na (pH 7.3, 290 mOsm). BLA neurons were voltage clamped at -70 mV to assess the excitatory postsynaptic currents (EPSCs) in response to presynaptic electrical or optogenetic stimulations. Concentric bipolar electrodes (FHC, Bowdoin, ME) or glass pipettes (~ 2 M Ω) filled with the extracellular solution were used as stimulating electrodes and placed on the external and internal capsules to evoke glutamate release in the BLA from cortical and thalamic axon terminals, respectively (Shin et al., 2010). A range of electrical pulses (intensities = 30 – 120 μ A, duration = 100 μ s) were delivered through a stimulator (Digitimer, UK) to evoke glutamate release at either cortical or thalamic inputs. To study the process of synaptic vesicle pool mobilization during repetitive glutamatergic transmission, we delivered 300 electrical pulses (duration = 100 μ s) at 12.5 Hz and measured the amplitudes of EPSCs to quantify changes in the

presynaptic glutamate release (Cabin et al., 2002). Only one neuron was recorded from each slice in the prolonged repetitive stimulation studies.

Optogenetic stimulation pulses (1 ms duration) were delivered through a 60x objective lens (Olympus, Japan) using a 470 nm LED light source (CoolLED, UK). To isolate monosynaptic cortico-BLA and thalamo-BLA EPSCs, optogenetically evoked EPSCs were recorded in the presence of TTX (1 μ M) and 4-AP (100 μ M). Series resistance (R_s , < 20 M Ω) was regularly monitored throughout the recording to ensure R_s changes were less than 15%. Liquid junction potential (~ 9 mV) was not corrected. Details of the protocol can be found at: <https://www.protocols.io/view/protocol-for-obtaining-rodent-brain-slices-for-ele-ewov1y7mpvr2/v2>.

Data analysis and statistics.

Electrophysiology data were analyzed offline in Clampfit 11.1 (RRID:SCR_011323, Molecular Devices, <http://www.moleculardevices.com/products/software/pclamp.html>). The peak amplitude of monosynaptic EPSCs in response to electric stimulation was quantified from an average of three to five sweeps. Digital confocal images were analyzed using ImageJ (RRID:SCR_003070, NIH, <https://imagej.net/>) or Imaris (RRID:SCR_007370, Oxford, UK, <http://www.bitplane.com/imaris/imaris>). Statistics were performed using Prism9 (RRID:SCR_002798, GraphPad Software, <http://www.graphpad.com/>). Non-parametric, distribution-independent Mann–Whitney U (MWU) test was used for non-paired data comparisons between groups, followed by Bonferroni-Dunn correction for multiple comparisons. Data from *Snca*^{SNL/SNL} mice were compared using one-way AVOVA (Šídák's multiple comparisons test). All tests were

612 two-tailed, and p value < 0.05 was considered statistically significant. Summary results
613 are reported as mean plus standard error of mean.

614 *Data availability.*

615 All tabular data associated with this study have been deposited on the Open Science
616 Framework (https://osf.io/jb6fn/?view_only=b338f3dc6ff1489eac332e9efdd86eb9).

617

References

- Abbott, L.F., and Regehr, W.G. (2004). Synaptic computation. *Nature* 431, 796–803.
<https://doi.org/10.1038/nature03010>.
- Abbott, L.F., Varela, J.A., Sen, K., and Nelson, S.B. (1997). Synaptic Depression and Cortical Gain Control. *Science* 275, 221–224.
<https://doi.org/10.1126/science.275.5297.221>.
- Abeliovich, A., Schmitz, Y., Fariñas, I., Choi-Lundberg, D., Ho, W.-H., Castillo, P.E., Shinsky, N., Verdugo, J.M.G., Armanini, M., Ryan, A., et al. (2000). Mice Lacking α -Synuclein Display Functional Deficits in the Nigrostriatal Dopamine System. *Neuron* 25, 239–252. [https://doi.org/10.1016/s0896-6273\(00\)80886-7](https://doi.org/10.1016/s0896-6273(00)80886-7).
- Ahmed, N., Headley, D.B., and Paré, D. (2021). Optogenetic study of central medial and paraventricular thalamic projections to the basolateral amygdala. *J Neurophysiol* 126, 1234–1247. <https://doi.org/10.1152/jn.00253.2021>.
- Alabi, A.A., and Tsien, R.W. (2012). Synaptic Vesicle Pools and Dynamics. *Csh Perspect Biol* 4, a013680. <https://doi.org/10.1101/cshperspect.a013680>.
- Amir, A., Paré, J., Smith, Y., and Paré, D. (2019). Midline thalamic inputs to the amygdala: Ultrastructure and synaptic targets. *J Comp Neurol* 527, 942–956.
<https://doi.org/10.1002/cne.24557>.
- Angot, E., Steiner, J.A., Hansen, C., Li, J.-Y., and Brundin, P. (2010). Are synucleinopathies prion-like disorders? *Lancet Neurology* 9, 1128–1138.
[https://doi.org/10.1016/s1474-4422\(10\)70213-1](https://doi.org/10.1016/s1474-4422(10)70213-1).
- Benskey, M.J., Perez, R.G., and Manfredsson, F.P. (2016). The contribution of alpha synuclein to neuronal survival and function – Implications for Parkinson's disease. *J Neurochem* 137, 331–359. <https://doi.org/10.1111/jnc.13570>.
- Bowers, D., Miller, K., Mikos, A., Kirsch-Darrow, L., Springer, U., Fernandez, H., Foote, K., and Okun, M. (2006). Startling facts about emotion in Parkinson's disease: blunted reactivity to aversive stimuli. *Brain* 129, 3356–3365.
<https://doi.org/10.1093/brain/awl301>.
- Buck, S.A., Miranda, B.R.D., Logan, R.W., Fish, K.N., Greenamyre, J.T., and Freyberg, Z. (2021). VGLUT2 Is a Determinant of Dopamine Neuron Resilience in a Rotenone Model of Dopamine Neurodegeneration. *J Neurosci* 41, 4937–4947.
<https://doi.org/10.1523/jneurosci.2770-20.2021>.

651 Burré, J., Sharma, M., Tsetsenis, T., Buchman, V., Etherton, M.R., and Südhof, T.C.
652 (2010). α -Synuclein Promotes SNARE-Complex Assembly in Vivo and in Vitro. *Science*
653 329, 1663–1667. <https://doi.org/10.1126/science.1195227>.

654 Burtscher, J., Copin, J.-C., Rodrigues, J., Kumar, S.T., Chiki, A., Suduiraut, M.-I.G. de,
655 Sandi, C., and Lashuel, H.A. (2019). Chronic corticosterone aggravates behavioural and
656 neuronal symptomatology in a mouse model of alpha-synuclein pathology. *Neurobiol*
657 *Aging* 83, 11–20. <https://doi.org/10.1016/j.neurobiolaging.2019.08.007>.

658 Cabin, D.E., Shimazu, K., Murphy, D., Cole, N.B., Gottschalk, W., McIlwain, K.L.,
659 Orrison, B., Chen, A., Ellis, C.E., Paylor, R., et al. (2002). Synaptic Vesicle Depletion
660 Correlates with Attenuated Synaptic Responses to Prolonged Repetitive Stimulation in
661 Mice Lacking α -Synuclein. *J Neurosci* 22, 8797–8807.
662 <https://doi.org/10.1523/jneurosci.22-20-08797.2002>.

663 Cookson, M.R., and Brug, M. van der (2008). Cell systems and the toxic mechanism(s)
664 of α -synuclein. *Exp Neurol* 209, 5–11. <https://doi.org/10.1016/j.expneurol.2007.05.022>.

665 Erskine, D., Patterson, L., Alexandris, A., Hanson, P.S., McKeith, I.G., Attems, J., and
666 Morris, C.M. (2018). Regional levels of physiological α -synuclein are directly associated
667 with Lewy body pathology. *Acta Neuropathol* 135, 153–154.
668 <https://doi.org/10.1007/s00401-017-1787-6>.

669 Fremeau, R.T., Troyer, M.D., Pahner, I., Nygaard, G.O., Tran, C.H., Reimer, R.J.,
670 Bellocchio, E.E., Fortin, D., Storm-Mathisen, J., and Edwards, R.H. (2001). The
671 Expression of Vesicular Glutamate Transporters Defines Two Classes of Excitatory
672 Synapse. *Neuron* 31, 247–260. [https://doi.org/10.1016/s0896-6273\(01\)00344-0](https://doi.org/10.1016/s0896-6273(01)00344-0).

673 Geertsma, H.M., Suk, T.R., Ricke, K.M., Horsthuis, K., Parmasad, J.-L.A., Fisk, Z.A.,
674 Callaghan, S.M., and Rousseaux, M.W.C. (2022). Constitutive nuclear accumulation of
675 endogenous alpha-synuclein in mice causes motor impairment and cortical dysfunction,
676 independent of protein aggregation. *Hum Mol Genet*
677 <https://doi.org/10.1093/hmg/ddac035>.

678 Harding, A.J., Stimson, E., Henderson, J.M., and Halliday, G.M. (2002). Clinical
679 correlates of selective pathology in the amygdala of patients with Parkinson's disease.
680 *Brain J Neurology* 125, 2431–2445. <https://doi.org/10.1093/brain/awf251>.

681 Henderson, M.X., Cornblath, E.J., Darwich, A., Zhang, B., Brown, H., Gathagan, R.J.,
682 Sandler, R.M., Bassett, D.S., Trojanowski, J.Q., and Lee, V.M.Y. (2019). Spread of α -
683 synuclein pathology through the brain connectome is modulated by selective
684 vulnerability and predicted by network analysis. *Nat Neurosci* 22, 1248–1257.
685 <https://doi.org/10.1038/s41593-019-0457-5>.

686 Hintiryan, H., Bowman, I., Johnson, D.L., Korobkova, L., Zhu, M., Khanjani, N., Gou, L.,
687 Gao, L., Yamashita, S., Bienkowski, M.S., et al. (2021). Connectivity characterization of

688 the mouse basolateral amygdalar complex. *Nat Commun* 12, 2859.
689 <https://doi.org/10.1038/s41467-021-22915-5>.

690 Hu, X., Song, X., Yuan, Y., Li, E., Liu, J., Liu, W., and Liu, Y. (2015). Abnormal
691 functional connectivity of the amygdala is associated with depression in Parkinson's
692 disease. *Movement Disord* 30, 238–244. <https://doi.org/10.1002/mds.26087>.

693 Janak, P.H., and Tye, K.M. (2015). From circuits to behaviour in the amygdala. *Nature*
694 517, 284–292. <https://doi.org/10.1038/nature14188>.

695 Kaneko, T., and Fujiyama, F. (2002). Complementary distribution of vesicular glutamate
696 transporters in the central nervous system. *Neurosci Res* 42, 243–250.
697 [https://doi.org/10.1016/s0168-0102\(02\)00009-3](https://doi.org/10.1016/s0168-0102(02)00009-3).

698 Luk, K.C., Song, C., O'Brien, P., Stieber, A., Branch, J.R., Brunden, K.R., Trojanowski,
699 J.Q., and Lee, V.M.-Y. (2009). Exogenous α -synuclein fibrils seed the formation of Lewy
700 body-like intracellular inclusions in cultured cells. *Proc National Acad Sci USA* 106,
701 20051–20056. <https://doi.org/10.1073/pnas.0908005106>.

702 Luk, K.C., Kehm, V., Carroll, J., Zhang, B., O'Brien, P., Trojanowski, J.Q., and Lee,
703 V.M.-Y. (2012). Pathological α -Synuclein Transmission Initiates Parkinson-like
704 Neurodegeneration in Nontransgenic Mice. *Science* 338, 949–953.
705 <https://doi.org/10.1126/science.1227157>.

706 Mezey, E., Dehejia, A.M., Harta, G., Suchy, S.F., Nussbaum, R.L., Brownstein, M.J.,
707 and Polymeropoulos, M.H. (1998). Alpha synuclein is present in Lewy bodies in
708 sporadic Parkinson's disease. *Mol Psychiatr* 3, 493–499.
709 <https://doi.org/10.1038/sj.mp.4000446>.

710 Nelson, P.T., Abner, E.L., Patel, E., Anderson, S., Wilcock, D.M., Kryscio, R.J., Eldik,
711 L.J.V., Jicha, G.A., Gal, Z., Nelson, R.S., et al. (2017). The Amygdala as a Locus of
712 Pathologic Misfolding in Neurodegenerative Diseases. *J Neuropathology Exp Neurology*
713 77, 2–20. <https://doi.org/10.1093/jnen/nlx099>.

714 Peng, C., Gathagan, R.J., Covell, D.J., Medellin, C., Stieber, A., Robinson, J.L., Zhang,
715 B., Pitkin, R.M., Olufemi, M.F., Luk, K.C., et al. (2018). Cellular milieu imparts distinct
716 pathological α -synuclein strains in α -synucleinopathies. *Nature* 557, 558–563.
717 <https://doi.org/10.1038/s41586-018-0104-4>.

718 Runwal, G., and Edwards, R.H. (2021). The Membrane Interactions of Synuclein:
719 Physiology and Pathology. *Annu Rev Pathology Mech Dis* 16, 465–485.
720 <https://doi.org/10.1146/annurev-pathol-031920-092547>.

721 Shin, R.-M., Tully, K., Li, Y., Cho, J.-H., Higuchi, M., Suhara, T., and Bolshakov, V.Y.
722 (2010). Hierarchical order of coexisting pre- and postsynaptic forms of long-term

723 potentiation at synapses in amygdala. *Proc National Acad Sci* 107, 19073–19078.
724 <https://doi.org/10.1073/pnas.1009803107>.

725 Sigurðsson, T., Sigurdsson, T., Cain, C.K., Doyère, V., and LeDoux, J.E. (2010).
726 Asymmetries in long-term and short-term plasticity at thalamic and cortical inputs to the
727 amygdala in vivo. *Eur J Neurosci* 31, 250–262. [https://doi.org/10.1111/j.1460-](https://doi.org/10.1111/j.1460-9568.2009.07056.x)
728 9568.2009.07056.x.

729 Sorrentino, Z.A., Goodwin, M.S., Riffe, C.J., Dhillon, J.-K.S., Xia, Y., Gorion, K.-M.,
730 Vijayaraghavan, N., McFarland, K.N., Golbe, L.I., Yachnis, A.T., et al. (2019). Unique α -
731 synuclein pathology within the amygdala in Lewy body dementia: implications for
732 disease initiation and progression. *Acta Neuropathologica Commun* 7, 142.
733 <https://doi.org/10.1186/s40478-019-0787-2>.

734 Spillantini, M.G., Schmidt, M.L., Lee, V.M.-Y., Trojanowski, J.Q., Jakes, R., and Goedert,
735 M. (1997). α -Synuclein in Lewy bodies. *Nature* 388, 839–840.
736 <https://doi.org/10.1038/42166>.

737 Stirling, D.R., Carpenter, A.E., and Cimini, B.A. (2021). CellProfiler Analyst 3.0:
738 Accessible data exploration and machine learning for image analysis. *Bioinformatics* 37,
739 btab634-. <https://doi.org/10.1093/bioinformatics/btab634>.

740 Stoyka, L.E., Arrant, A.E., Thrasher, D.R., Russell, D.L., Freire, J., Mahoney, C.L.,
741 Narayanan, A., Dib, A.G., Standaert, D.G., and Volpicelli-Daley, L.A. (2019). Behavioral
742 defects associated with amygdala and cortical dysfunction in mice with seeded α -
743 synuclein inclusions. *Neurobiol Dis* 104708. <https://doi.org/10.1016/j.nbd.2019.104708>.

744 Sulzer, D., and Edwards, R.H. (2019). The physiological role of α -synuclein and its
745 relationship to Parkinson's Disease. *J Neurochem* 150, 475–486.
746 <https://doi.org/10.1111/jnc.14810>.

747 Surmeier, D.J., Obeso, J.A., and Halliday, G.M. (2017). Selective neuronal vulnerability
748 in Parkinson disease. *Nat Rev Neurosci* 18, 101–113.
749 <https://doi.org/10.1038/nrn.2016.178>.

750 Taguchi, K., Watanabe, Y., Tsujimura, A., and Tanaka, M. (2015). Brain region-
751 dependent differential expression of alpha-synuclein. *J Comp Neurol* 524, 1236–1258.
752 <https://doi.org/10.1002/cne.23901>.

753 Thakur, P., Chiu, W.H., Roeper, J., and Goldberg, J.A. (2019). α -SYNUCLEIN 2.0 –
754 Moving towards Cell-Type Specific Pathophysiology. *Neuroscience* 412, 248–256.
755 <https://doi.org/10.1016/j.neuroscience.2019.06.005>.

756 Thomas, S., S, C., William, Imre, K., A, R., Robert, B, L., Edward, Q, T., John, Zachary,
757 F., Subhojit, R., C, L., Kelvin, M, L., Virginia, et al. (2021). Dopamine neurons exhibit

758 emergent glutamatergic identity in Parkinson's disease. *Brain* awab373.
759 <https://doi.org/10.1093/brain/awab373>.

760 Uemura, N., Uemura, M.T., Luk, K.C., Lee, V.M.-Y., and Trojanowski, J.Q. (2020). Cell-
761 to-Cell Transmission of Tau and α -Synuclein. *Trends Mol Med* 26, 936–952.
762 <https://doi.org/10.1016/j.molmed.2020.03.012>.

763 Vargas, K.J., Schrod, N., Davis, T., Fernandez-Busnadiego, R., Taguchi, Y.V., Laugks,
764 U., Lucic, V., and Chandra, S.S. (2017). Synucleins Have Multiple Effects on
765 Presynaptic Architecture. *Cell Reports* 18, 161–173.
766 <https://doi.org/10.1016/j.celrep.2016.12.023>.

767 Vasili, E., Dominguez-Meijide, A., Flores-León, M., Al-Azzani, M., Kanellidi, A., Melki, R.,
768 Stefanis, L., and Outeiro, T.F. (2022). Endogenous Levels of Alpha-Synuclein Modulate
769 Seeding and Aggregation in Cultured Cells. *Mol Neurobiol* 1–12.
770 <https://doi.org/10.1007/s12035-021-02713-2>.

771 Vigneault, É., Poirel, O., Riad, M., Prud'homme, J., Dumas, S., Turecki, G., Fasano, C.,
772 Mechawar, N., and Mestikawy, S.E. (2015). Distribution of vesicular glutamate
773 transporters in the human brain. *Front Neuroanat* 9, 23.
774 <https://doi.org/10.3389/fnana.2015.00023>.

775 Volpicelli-Daley, L.A., Luk, K.C., Patel, T.P., Tanik, S.A., Riddle, D.M., Stieber, A.,
776 Meaney, D.F., Trojanowski, J.Q., and Lee, V.M.-Y. (2011). Exogenous α -Synuclein
777 Fibrils Induce Lewy Body Pathology Leading to Synaptic Dysfunction and Neuron Death.
778 *Neuron* 72, 57–71. <https://doi.org/10.1016/j.neuron.2011.08.033>.

779 Volpicelli-Daley, L.A., Luk, K.C., and Lee, V.M.-Y. (2014). Addition of exogenous α -
780 synuclein preformed fibrils to primary neuronal cultures to seed recruitment of
781 endogenous α -synuclein to Lewy body and Lewy neurite-like aggregates. *Nat Protoc* 9,
782 2135–2146. <https://doi.org/10.1038/nprot.2014.143>.

783 West, M.J. (1999). Stereological methods for estimating the total number of neurons
784 and synapses: issues of precision and bias. *Trends Neurosci* 22, 51–61.
785 [https://doi.org/10.1016/s0166-2236\(98\)01362-9](https://doi.org/10.1016/s0166-2236(98)01362-9).

786 Yoshimura, N., Kawamura, M., Masaoka, Y., and Homma, I. (2005). The amygdala of
787 patients with Parkinson's disease is silent in response to fearful facial expressions.
788 *Neuroscience* 131, 523–534. <https://doi.org/10.1016/j.neuroscience.2004.09.054>.

789 Ziolkowska, B., Gieryk, A., Bilecki, W., Wawrzczak-Bargiela, A., Wedzony, K., Chocyk,
790 A., Danielson, P.E., Thomas, E.A., Hilbush, B.S., Sutcliffe, J.G., et al. (2005).
791 Regulation of α -Synuclein Expression in Limbic and Motor Brain Regions of Morphine-
792 Treated Mice. *J Neurosci* 25, 4996–5003. [https://doi.org/10.1523/jneurosci.4376-](https://doi.org/10.1523/jneurosci.4376-04.2005)
793 04.2005.

